



Article

# Compounding $\text{MgCl}_2 \cdot 6\text{H}_2\text{O}$ with $\text{NH}_4\text{Al}(\text{SO}_4)_2 \cdot 12\text{H}_2\text{O}$ or $\text{KAl}(\text{SO}_4)_2 \cdot 12\text{H}_2\text{O}$ to Obtain Binary Hydrated Salts as High-Performance Phase Change Materials

Wanchun Sun<sup>1</sup>, Yan Zhou<sup>1</sup>, Jinxin Feng<sup>1</sup>, Xiaoming Fang<sup>1,2</sup>, Ziyi Ling<sup>1,2,\*</sup>  and Zhengguo Zhang<sup>1,2,\*</sup> 

<sup>1</sup> Key Laboratory of Enhanced Heat Transfer and Energy Conservation, The Ministry of Education, School of Chemistry and Chemical Engineering, South China University of Technology, Guangzhou 510640, China; greycici1114@gmail.com (W.S.); zhouyanscut@163.com (Y.Z.); cefjxfeng@mail.scut.edu.cn (J.F.); cexmfang@scut.edu.cn (X.F.)

<sup>2</sup> Guangdong Engineering Technology Research Center of Efficient Heat Storage and Application, South China University of Technology, Guangzhou 510640, China

\* Correspondence: zyiling@scut.edu.cn (Z.L.); cezhang@scut.edu.cn (Z.Z.); Tel.: +86-20-8711-2845 (Z.L. & Z.Z.); Fax: +86-20-8711-3870 (Z.L. & Z.Z.)

Received: 21 December 2018; Accepted: 19 January 2019; Published: 21 January 2019



**Abstract:** Developing phase change materials (PCMs) with suitable phase change temperatures and high latent heat is of great significance for accelerating the development of latent heat storage technology to be applied in solar water heating (SWH) systems. The phase change performances of two mixtures,  $\text{NH}_4\text{Al}(\text{SO}_4)_2 \cdot 12\text{H}_2\text{O} \cdot \text{MgCl}_2 \cdot 6\text{H}_2\text{O}$  (mixture-A) and  $\text{KAl}(\text{SO}_4)_2 \cdot 12\text{H}_2\text{O} \cdot \text{MgCl}_2 \cdot 6\text{H}_2\text{O}$  (mixture-B), were investigated in this paper. Based on the DSC results, the optimum contents of  $\text{MgCl}_2 \cdot 6\text{H}_2\text{O}$  in mixture-A and mixture-B were determined to be 30 wt%. It is found that the melting points of mixture-A (30 wt%  $\text{MgCl}_2 \cdot 6\text{H}_2\text{O}$ ) and mixture-B (30 wt%  $\text{MgCl}_2 \cdot 6\text{H}_2\text{O}$ ) are 64.15 °C and 60.15 °C, respectively, which are suitable for SWH systems. Moreover, two mixtures have high latent heat of up to 192.1 kJ/kg and 198.1 kJ/kg as well as exhibit little supercooling. After 200 cycles heating-cooling experiments, the deviations in melting point and melting enthalpy of mixture-A are only 1.51% and 1.20%, respectively. Furthermore, the XRD patterns before and after the cycling experiments show that mixture-A possesses good structure stability. These excellent thermal characteristics make mixture-A show great potential for SWH systems.

**Keywords:** latent heat storage; phase change material; magnesium chloride hexahydrate; aluminum ammonium sulfate dodecahydrate; aluminum potassium sulfate dodecahydrate

## 1. Introduction

Thermal energy storage (TES) is a key technology for improving energy efficiency and developing solar energy, since it can solve the mismatch between heat supply and demand in space and time [1–3]. Sensible thermal energy storage (STES), latent thermal energy storage (LTES) and thermo-chemical heat storage (TCHS) are the main approaches to realize TES [4]. Compared to STES and TCHS, LTES using phase change materials (PCMs) has attracted increasing interest because of high energy storage density [5]. PCM can absorb or release a large amount of heat during the phase change process while maintaining the system at a constant temperature around its melting point [6]. In order to further enhance the heat storage performance of LTES, PCM should possess the merits of large latent heat, good thermal stability and excellent thermal reliability. Moreover, it is desirable in industrial

applications that PCM has a low cost and a suitable phase change temperature for target thermal system. Therefore, the exploration of PCMs that meet the above requirements is of great significance for accelerating the latent heat storage technology to be applied into various fields.

In general, PCMs can be classified into two types: organics and inorganics. Organic PCMs, such as paraffin waxes [7], fatty acids [8], and fatty alcohols [9], have the advantages of little supercooling, no phase separation and non-corrosiveness [10]. However, low thermal conductivity, relatively low phase change enthalpy, large volume change during phase transition and high price limit the widespread use of organic PCMs [11]. By comparison, inorganic PCMs have the advantages of low cost, incombustibility, large latent heat and relatively high thermal conductivity, making them show great potential for application [12]. Inorganic PCMs can be further classified into hydrated salts, molten salts and metals, which are suitable for use in low, medium and high-temperature application fields [13,14]. As a major PCM used in low-temperature environment, hydrated salts show great potential uses in various fields, such as solar water heating (SWH) systems [15], heating and cooling buildings [16], off-peak power utilization [17], heat pump water heating systems, etc. [18]. Nevertheless, the supercooling phenomenon, phase separation and poor thermal reliability of hydrated salts have become unavoidable problems that needs to be solved urgently. For the better applications of hydrated salts, it is necessary to develop an inorganic PCM with high latent heat, good thermal stability and thermal reliability, and low supercooling degree.

In recent years, enormous amounts of research have been carried out on solutions to the disadvantages of hydrated salts. In order to reduce the supercooling degree, the study on the nucleating agents for different hydrated salts has been strongly promoted. Lane [19] conducted experiments to evaluate different nucleating agents for calcium chloride hexahydrate ( $\text{CaCl}_2 \cdot 6\text{H}_2\text{O}$ ). The experimental results showed that  $\text{BaI}_2 \cdot 6\text{H}_2\text{O}$ ,  $\text{SrCl}_2 \cdot 6\text{H}_2\text{O}$ , and  $\text{SrBr}_2 \cdot 6\text{H}_2\text{O}$  could effectively suppress the supercooling of  $\text{CaCl}_2 \cdot 6\text{H}_2\text{O}$ . As for sodium acetate trihydrate, the introduction of aluminum nitride [20], silver nanoparticles [21],  $\text{Si}_3\text{N}_4$ ,  $\text{ZrB}_2$  and  $\text{SiO}_2$  [22] were all proven to be able to effectively reduce the supercooling degree. On the other hand, the phase separation of hydrated salts can be solved by adding thickeners, such as hydroxyethyl cellulose (HEC) [19,23] and carboxymethylcellulose sodium (CMC) [20,24–26]. Furthermore, the combination of porous carriers and hydrated salts can mitigate the negative effects of the phase separation and improve the thermal reliability of the hydrated salts. Due to the large specific surface area, expanded graphite [27,28], expanded perlite [29,30] and diatomite [31,32] were widely used for the preparation of stable composites. In addition to the addition of nucleating agents and thickeners and the combination with porous carriers, a mixture composed of two or more hydrated salts have attracted the attention of more and more scholars. In some hydrated salt systems, mixing with other hydrated salts can not only adjust the melting point, but also reduce the supercooling degree and mitigate phase separation. Nagano et al. [33] added 20 wt%  $\text{MgCl}_2 \cdot 6\text{H}_2\text{O}$  to  $\text{MgNO}_3 \cdot 6\text{H}_2\text{O}$  to obtain a eutectic mixture. They reported that the mixture exhibited a melting point of about 60 °C, which was much lower than those of two components and was suitable for recovering waste heat. Moreover, Li et al. [23] investigated the  $\text{CaCl}_2 \cdot 6\text{H}_2\text{O}$ - $\text{MgCl}_2 \cdot 6\text{H}_2\text{O}$  salt system with various mass fraction of  $\text{MgCl}_2 \cdot 6\text{H}_2\text{O}$ . It was found that the mixing of two hydrated salts not only reduced the melting point of  $\text{CaCl}_2 \cdot 6\text{H}_2\text{O}$  but also retained most of the melting enthalpy. Note that hydrated salt mixtures usually exhibit different phase change temperatures and latent heat values from those of their components [34]. Therefore, exploration of mixtures is an effective route for developing novel hydrated salt PCMs. According to the requirements of SWH systems, such as suitable melting point, low cost and excellent performance, the mixtures with high latent heat and appropriate phase change temperatures are highly desirable.

In the current work, two hydrated mixtures were explored by combining aluminum ammonium sulfate dodecahydrate ( $\text{NH}_4\text{Al}(\text{SO}_4)_2 \cdot 12\text{H}_2\text{O}$ ) or aluminum potassium sulfate dodecahydrate ( $\text{KAl}(\text{SO}_4)_2 \cdot 12\text{H}_2\text{O}$ ) with magnesium chloride hexahydrate ( $\text{MgCl}_2 \cdot 6\text{H}_2\text{O}$ ).  $\text{MgCl}_2 \cdot 6\text{H}_2\text{O}$  is a hydrated salt with a melting point of 117 °C and a melting enthalpy of about 150 kJ/kg. Owing to the abundant

magnesium chloride resources in salt lakes,  $\text{MgCl}_2 \cdot 6\text{H}_2\text{O}$  is an ideal low-cost PCM. But the high melting point ( $117\text{ }^\circ\text{C}$ ) influences the thermal stability and reliability of  $\text{MgCl}_2 \cdot 6\text{H}_2\text{O}$  because it is higher than the boiling point of water ( $100\text{ }^\circ\text{C}$ , at standard atmospheric pressure). On the other hand,  $\text{NH}_4\text{Al}(\text{SO}_4)_2 \cdot 12\text{H}_2\text{O}$  and  $\text{KAl}(\text{SO}_4)_2 \cdot 12\text{H}_2\text{O}$  are common hydrated salts in daily life with phase change temperatures of about  $93\text{ }^\circ\text{C}$  and latent heat of up to  $260\text{ kJ/kg}$ . However, the large supercooling degree ( $10\text{--}15\text{ }^\circ\text{C}$ ) and relatively high phase change temperature limit their practical application in SWH systems. In order to reduce the melting point of  $\text{NH}_4\text{Al}(\text{SO}_4)_2 \cdot 12\text{H}_2\text{O}$  or  $\text{KAl}(\text{SO}_4)_2 \cdot 12\text{H}_2\text{O}$  as well as retain the high melting enthalpy, two series of mixtures consisting of  $\text{MgCl}_2 \cdot 6\text{H}_2\text{O}$  and  $\text{NH}_4\text{Al}(\text{SO}_4)_2 \cdot 12\text{H}_2\text{O}$  or  $\text{KAl}(\text{SO}_4)_2 \cdot 12\text{H}_2\text{O}$  were prepared by a melt blending method. The introduction of  $\text{MgCl}_2 \cdot 6\text{H}_2\text{O}$  was expected to adjust the thermal properties of  $\text{NH}_4\text{Al}(\text{SO}_4)_2 \cdot 12\text{H}_2\text{O}$  or  $\text{KAl}(\text{SO}_4)_2 \cdot 12\text{H}_2\text{O}$  to obtain a mixture that meet the requirements of ideal PCM. For determining the compositions of mixtures, the influences of the mass fraction of  $\text{MgCl}_2 \cdot 6\text{H}_2\text{O}$  were studied. Furthermore, the obtained mixtures were characterized by various techniques, and their thermal reliabilities were evaluated to provide better guidance for industrial applications.

## 2. Results and Discussion

### 2.1. Determining the Mixture Composition

In order to describe the experimental results clearly, the mixtures were classified into 2 series, as shown in Table 1. Figure 1 shows the molten mixtures including mixtures-A and mixtures-B with different mass fractions of  $\text{MgCl}_2 \cdot 6\text{H}_2\text{O}$  ( $F_{\text{MgCl}_2 \cdot 6\text{H}_2\text{O}}$ ). It can be seen from Figure 1a that mixtures-A containing 30% and 40%  $\text{MgCl}_2 \cdot 6\text{H}_2\text{O}$  show transparent and semitransparent solutions, while others are in solid state. On the other hand, mixtures-B containing 30%, 40% and 50%  $\text{MgCl}_2 \cdot 6\text{H}_2\text{O}$  are semitransparent solutions, as shown in Figure 1b. To investigate the effect of  $F_{\text{MgCl}_2 \cdot 6\text{H}_2\text{O}}$  on the thermal properties of mixture-A/mixtures-B, the melting point ( $T_{\text{melt}}$ ) and enthalpy ( $\Delta H$ ) of each sample was measured by DSC (as shown in Figure 2a,c). The thermal characteristics of mixtures-A/mixtures-B are listed in Table 2. It can be seen that  $T_{\text{melt}}$  first increases then decreases with the increase of  $F_{\text{MgCl}_2 \cdot 6\text{H}_2\text{O}}$ . As for mixture-A/ mixture-B, when  $F_{\text{MgCl}_2 \cdot 6\text{H}_2\text{O}}$  exceeds 50 wt%,  $T_{\text{melt}}$  and  $\Delta H$  decrease significantly. The results show that there is an optimum mass fraction of  $\text{MgCl}_2 \cdot 6\text{H}_2\text{O}$  for mixture-A/mixture-B. It can be seen from the experimental results (Figure 1, Figure 2a,c, Table 2) that the optimum addition of  $\text{MgCl}_2 \cdot 6\text{H}_2\text{O}$  is between 20 wt% and 40 wt%. Therefore, mixtures-A/B containing 25 wt% and 35 wt%  $\text{MgCl}_2 \cdot 6\text{H}_2\text{O}$  were prepared and characterized by DSC to determine the optimum  $F_{\text{MgCl}_2 \cdot 6\text{H}_2\text{O}}$ . As shown in Figure 2b,d, mixture-A and mixture-B containing 30 wt% exhibit excellent thermal properties ( $\text{NH}_4\text{Al}(\text{SO}_4)_2 \cdot 12\text{H}_2\text{O}$ -30 wt%  $\text{MgCl}_2 \cdot 6\text{H}_2\text{O}$ :  $T_{\text{melt}} = 64.15\text{ }^\circ\text{C}$ ,  $\Delta H = 192.1\text{ kJ/kg}$ ;  $\text{KAl}(\text{SO}_4)_2 \cdot 12\text{H}_2\text{O}$  -30 wt%  $\text{MgCl}_2 \cdot 6\text{H}_2\text{O}$ :  $T_{\text{melt}} = 60.93\text{ }^\circ\text{C}$ ,  $\Delta H = 198.1\text{ kJ/kg}$ ), which are denoted as mixture-A and mixture-B for further research in this work, respectively.

Table 1. Different mixture series.

Mixture	Compositions	
A	$\text{MgCl}_2 \cdot 6\text{H}_2\text{O}$	$\text{NH}_4\text{Al}(\text{SO}_4)_2 \cdot 12\text{H}_2\text{O}$
B	$\text{MgCl}_2 \cdot 6\text{H}_2\text{O}$	$\text{KAl}(\text{SO}_4)_2 \cdot 12\text{H}_2\text{O}$

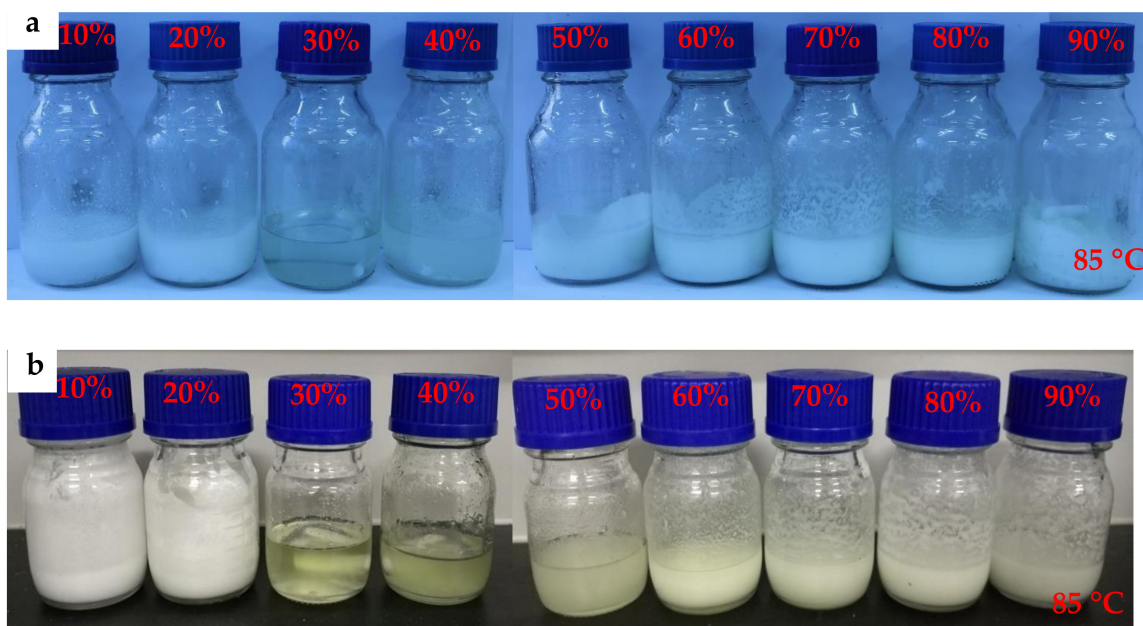


Figure 1. Photographs of (a) mixtures-A and (b) mixtures-B with different  $F_{MgCl_2 \cdot 6H_2O}$ .

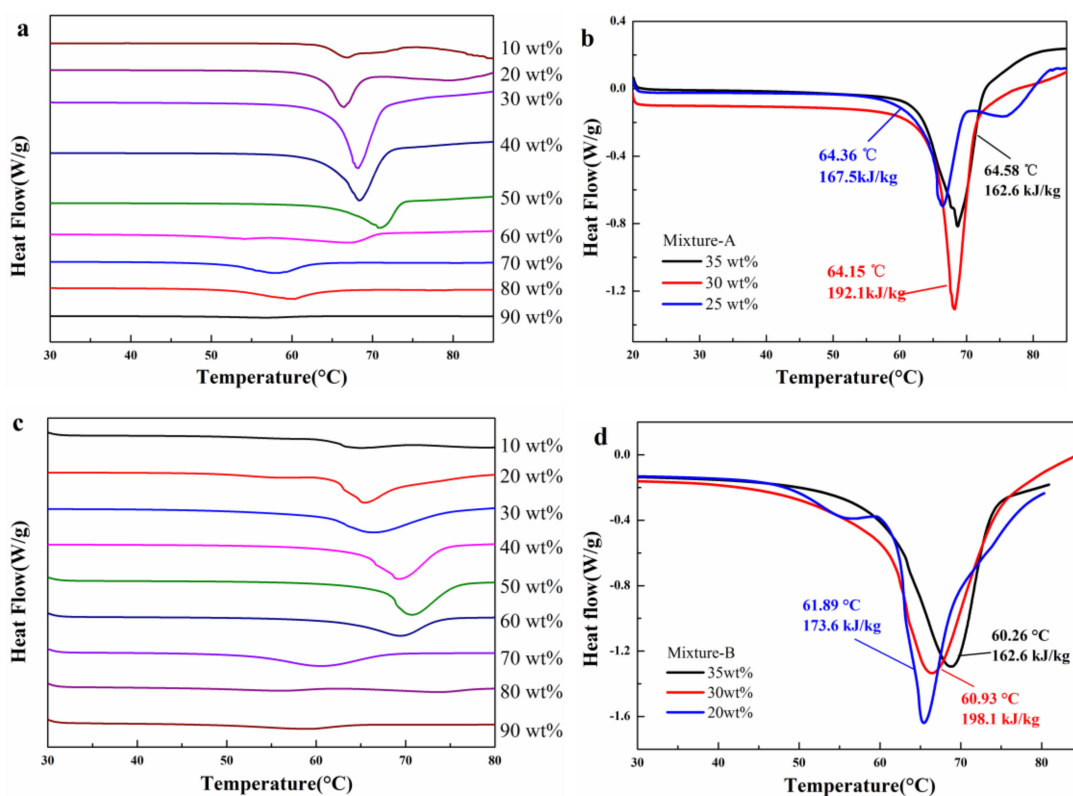


Figure 2. DSC curves of (a,b) mixtures-A and (c,d) mixtures-B with different  $F_{MgCl_2 \cdot 6H_2O}$ .

**Table 2.** Thermal characteristics of mixtures (mixture-A and mixture-B) with different mass fractions of  $\text{MgCl}_2 \cdot 6\text{H}_2\text{O}$  below 85 °C.

Mixture-A			Mixture-B		
$F_{\text{MgCl}_2 \cdot 6\text{H}_2\text{O}}$ <sup>1</sup> (wt%)	$T_{\text{melt}}$ (°C) <sup>2</sup>	$\Delta H$ (kJ/kg) <sup>3</sup>	$F_{\text{MgCl}_2 \cdot 6\text{H}_2\text{O}}$ (wt%)	$T_{\text{melt}}$ (°C)	$\Delta H$ (kJ/kg)
10	63.54	141.8	10	61.00	165.0
20	63.90	131.9	20	61.89	173.6
30	64.15	192.1	30	60.93	198.1
40	65.08	138.4	40	64.67	173.3
50	65.97	83.17	50	67.92	145.6
60	53.90	60.13	60	60.86	100.0
70	52.23	46.59	70	50.42	92.14
80	51.94	45.72	80	45.49	57.30
90	48.00	7.747	90	49.00	24.21

<sup>1</sup>  $F_{\text{MgCl}_2 \cdot 6\text{H}_2\text{O}}$ —the mass fraction of  $\text{MgCl}_2 \cdot 6\text{H}_2\text{O}$ ; <sup>2</sup>  $T_{\text{melt}}$ —the melting point of mixture; <sup>3</sup>  $\Delta H$ —the melting enthalpy of mixture.

## 2.2. Structure and Thermal Properties of the Mixtures

Figure 3 displays the polarized microscope images obtained at different times during crystallization. The  $\text{MgCl}_2 \cdot 6\text{H}_2\text{O}$  crystals are acicular, with sizes of 0.1–1  $\mu\text{m}$ . On the other hand,  $\text{NH}_4\text{Al}(\text{SO}_4)_2 \cdot 12\text{H}_2\text{O}$  and  $\text{KAl}(\text{SO}_4)_2 \cdot 12\text{H}_2\text{O}$  exhibit octahedral crystals with sizes of 100–150  $\mu\text{m}$ , which are much larger than those of  $\text{MgCl}_2 \cdot 6\text{H}_2\text{O}$ . In the first stage of the crystallization of mixture-A, a number of acicular crystals ( $\text{MgCl}_2 \cdot 6\text{H}_2\text{O}$ ) grow rapidly within 1 s. Some 70 s later, it can be seen that several octahedral crystals ( $\text{NH}_4\text{Al}(\text{SO}_4)_2 \cdot 12\text{H}_2\text{O}$ ) start to grow at a slow rate. Finally, the acicular crystals stick into the gaps among the octahedral crystals or attach to the surfaces of the octahedral crystals. As shown in the crystal image (Figure 3a, 320 s) of the mixture-A, two crystals with different shapes are tightly bound together to form the crystal of mixture A. Similarly, the acicular crystals ( $\text{MgCl}_2 \cdot 6\text{H}_2\text{O}$ ) grow rapidly during the crystallization of mixture-B. The octahedral crystals ( $\text{KAl}(\text{SO}_4)_2 \cdot 12\text{H}_2\text{O}$ ) begin to appear at 30 s and develop gradually. It can be seen from Figure 3b that the acicular crystals finally attach to the surfaces of the octahedral crystals. However, there is no connection of acicular crystal between two octahedral crystals.

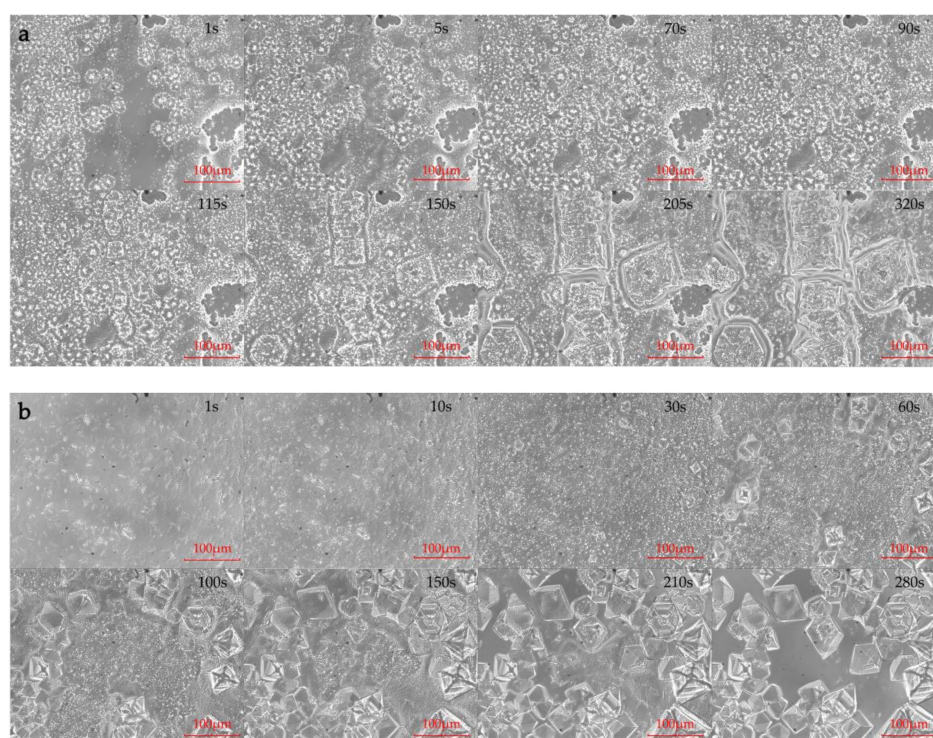
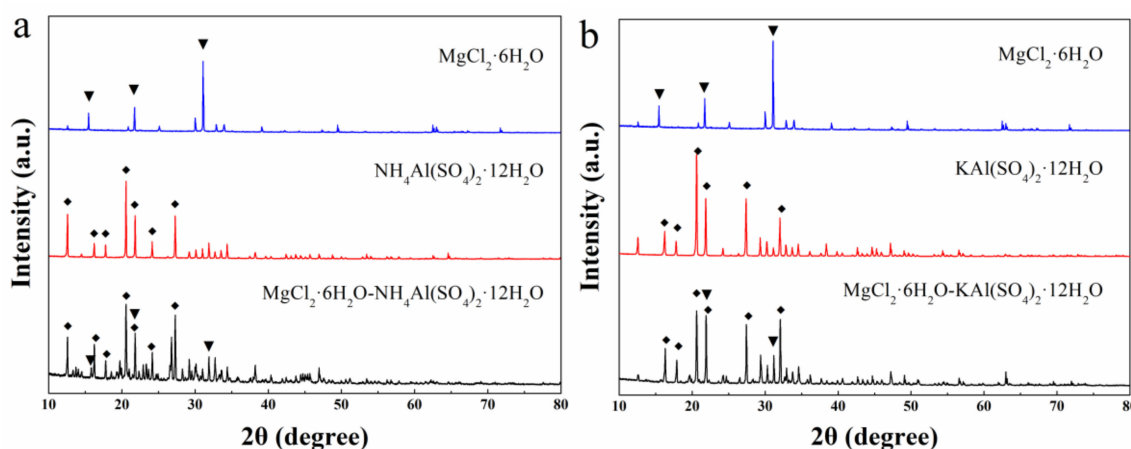
**Figure 3.** Polarized microscope images of (a) mixture-A and (b) mixture-B during crystallization.

Figure 4 displays the XRD patterns of  $\text{MgCl}_2 \cdot 6\text{H}_2\text{O}$ ,  $\text{NH}_4\text{Al}(\text{SO}_4)_2 \cdot 12\text{H}_2\text{O}$ ,  $\text{KAl}(\text{SO}_4)_2 \cdot 12\text{H}_2\text{O}$ , mixture-A (a) and mixture-B (b). It can be seen from Figure 4a that the XRD pattern of the mixture-A contains the diffraction peaks with strong intensities for  $\text{NH}_4\text{Al}(\text{SO}_4)_2 \cdot 12\text{H}_2\text{O}$  and the ones with low intensities for  $\text{MgCl}_2 \cdot 6\text{H}_2\text{O}$ . This is reasonable because the low content (30 wt%) of  $\text{MgCl}_2 \cdot 6\text{H}_2\text{O}$  in the mixture and the much smaller sizes of the  $\text{MgCl}_2 \cdot 6\text{H}_2\text{O}$  crystals comparing to those of  $\text{NH}_4\text{Al}(\text{SO}_4)_2 \cdot 12\text{H}_2\text{O}$  (Figure 3). It is revealed that the mixture is composed of  $\text{MgCl}_2 \cdot 6\text{H}_2\text{O}$  and  $\text{NH}_4\text{Al}(\text{SO}_4)_2 \cdot 12\text{H}_2\text{O}$ . Moreover, several new diffraction peaks with low intensities appear in the XRD pattern of the mixture, which might originate from the integrated crystals between  $\text{MgCl}_2 \cdot 6\text{H}_2\text{O}$  and  $\text{NH}_4\text{Al}(\text{SO}_4)_2 \cdot 12\text{H}_2\text{O}$ . Different from Figure 4a, only the diffraction peaks of  $\text{MgCl}_2 \cdot 6\text{H}_2\text{O}$  and  $\text{KAl}(\text{SO}_4)_2 \cdot 12\text{H}_2\text{O}$  are shown in the XRD pattern of mixture-B, and there is no new diffraction peak appears (Figure 4b). Therefore, the  $\text{MgCl}_2 \cdot 6\text{H}_2\text{O}$  and  $\text{KAl}(\text{SO}_4)_2 \cdot 12\text{H}_2\text{O}$  are only physically mixed without any chemical reaction in the preparation of the mixture-B.



**Figure 4.** XRD patterns of  $\text{MgCl}_2 \cdot 6\text{H}_2\text{O}$ ,  $\text{NH}_4\text{Al}(\text{SO}_4)_2 \cdot 12\text{H}_2\text{O}$ ,  $\text{KAl}(\text{SO}_4)_2 \cdot 12\text{H}_2\text{O}$  and (a) mixture-A; (b) mixture-B.

Figure 5 shows the DSC melting curves of  $\text{MgCl}_2 \cdot 6\text{H}_2\text{O}$ ,  $\text{NH}_4\text{Al}(\text{SO}_4)_2 \cdot 12\text{H}_2\text{O}$ ,  $\text{KAl}(\text{SO}_4)_2 \cdot 12\text{H}_2\text{O}$  and mixtures. As shown in Figure 5a,b, the melting points are measured to be 64.15 °C and 60.93 °C for mixture-A and mixture-B, respectively. The melting points are much lower than the boiling point of water (100 °C, at standard atmospheric pressure). It can be inferred that the mixtures do not suffer from the instability of being prone to lose crystal water during melting. Furthermore, the melting enthalpy are 192.1 kJ/kg and 198.1 kJ/kg for mixture-A and mixture-B, respectively. Compared to the eutectic salt containing  $\text{MgCl}_2 \cdot 6\text{H}_2\text{O}$  such as  $\text{MgCl}_2 \cdot 6\text{H}_2\text{O} \cdot \text{Mg}(\text{NO}_3)_2 \cdot 6\text{H}_2\text{O}$  and  $\text{MgCl}_2 \cdot 6\text{H}_2\text{O} \cdot \text{CaCl}_2 \cdot 6\text{H}_2\text{O}$  [23,33,35,36], mixture-A and mixture-B have much larger melting enthalpy. The suitable melting points (64.15 °C, 60.93 °C) and the large latent heat (192.1 kJ/kg, 198.1 kJ/kg) of mixture-A and mixture-B demonstrate their great potential in for solar water heating systems.

The cooling curves of  $\text{MgCl}_2 \cdot 6\text{H}_2\text{O}$ ,  $\text{NH}_4\text{Al}(\text{SO}_4)_2 \cdot 12\text{H}_2\text{O}$ ,  $\text{KAl}(\text{SO}_4)_2 \cdot 12\text{H}_2\text{O}$  and mixtures are displayed in Figure 6. The supercooling degree is found to be about 15.27 °C for  $\text{MgCl}_2 \cdot 6\text{H}_2\text{O}$ , 10.51 °C for  $\text{NH}_4\text{Al}(\text{SO}_4)_2 \cdot 12\text{H}_2\text{O}$  and 15.02 °C for  $\text{KAl}(\text{SO}_4)_2 \cdot 12\text{H}_2\text{O}$ . However, mixture-A exhibits a supercooling degree of 0.74 °C and mixture-B has no supercooling degree. The experimental results show that the combination of two hydrated salts ( $\text{MgCl}_2 \cdot 6\text{H}_2\text{O}$  and  $\text{NH}_4\text{Al}(\text{SO}_4)_2 \cdot 12\text{H}_2\text{O}$  or  $\text{KAl}(\text{SO}_4)_2 \cdot 12\text{H}_2\text{O}$ ) lead to a low supercooling degree for the mixture. Compared to  $\text{MgCl}_2 \cdot 6\text{H}_2\text{O}$ , mixture-A/mixture-B has a more suitable phase change temperature, higher melting enthalpy and lower supercooling degree. On the other hand, although the latent heat of  $\text{NH}_4\text{Al}(\text{SO}_4)_2 \cdot 12\text{H}_2\text{O}$  or  $\text{KAl}(\text{SO}_4)_2 \cdot 12\text{H}_2\text{O}$  is higher than that of mixture-A/mixture-B, the large supercooling degree greatly limits its practical applications. These results suggest that mixture-A and mixture-B show

greater promise for practical applications as compared with  $\text{MgCl}_2 \cdot 6\text{H}_2\text{O}$ ,  $\text{NH}_4\text{Al}(\text{SO}_4)_2 \cdot 12\text{H}_2\text{O}$  and  $\text{KAl}(\text{SO}_4)_2 \cdot 12\text{H}_2\text{O}$ .

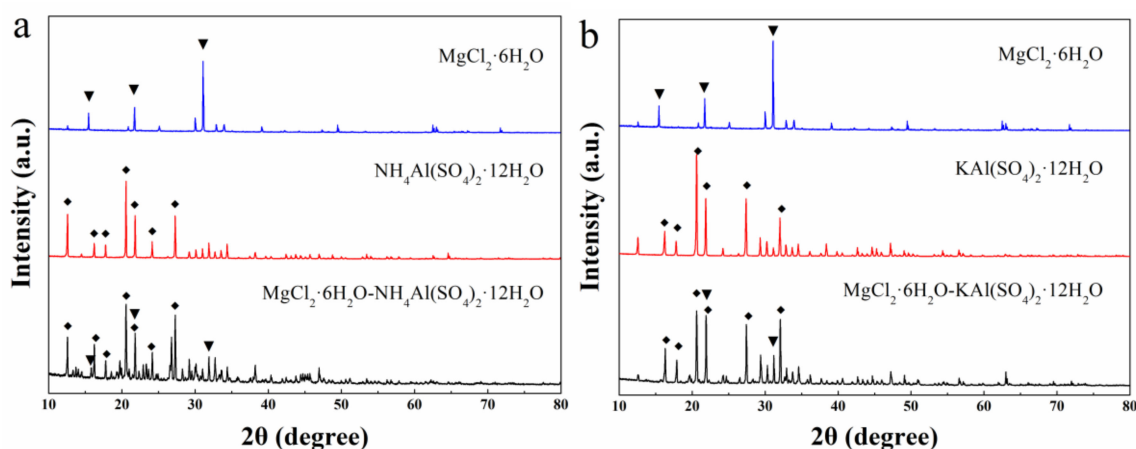


**Figure 5.** DSC curves of (a)  $\text{MgCl}_2 \cdot 6\text{H}_2\text{O}$ ,  $\text{NH}_4\text{Al}(\text{SO}_4)_2 \cdot 12\text{H}_2\text{O}$  and mixture-A; (b)  $\text{MgCl}_2 \cdot 6\text{H}_2\text{O}$ ,  $\text{KAl}(\text{SO}_4)_2 \cdot 12\text{H}_2\text{O}$  and mixture-B.

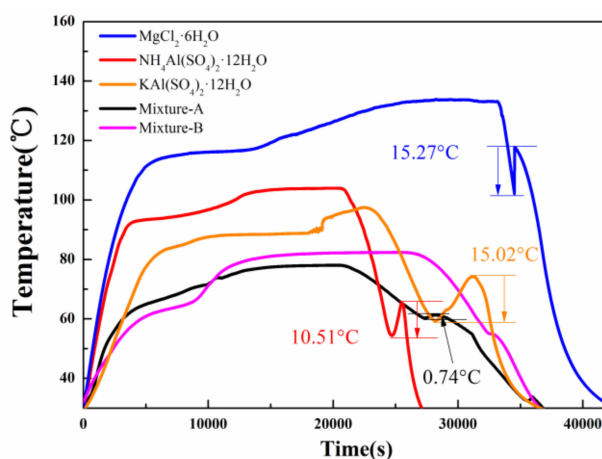


**Figure 6.** Cooling curves of three hydrated salts and mixture-A/B.

The thermal stability of the mixture was evaluated by TGA. Figure 7 illustrates the weight loss curves of three hydrated salts and mixture-A/B. For  $\text{MgCl}_2 \cdot 6\text{H}_2\text{O}$  (Figure 7a), it starts to decompose at about  $60^\circ\text{C}$  and the weight loss due to the adsorbed air humidity is about 4.25%. At the temperature of  $163.4^\circ\text{C}$ , the weight loss reach the second peak and the weight loss at this stage is 24.64%. After that, the product  $\text{MgCl}_2 \cdot 4\text{H}_2\text{O}$  starts to decompose, resulting in the maximum rate of water loss. The  $\text{MgCl}_2 \cdot 4\text{H}_2\text{O}$  lose two crystal waters and becomes  $\text{MgCl}_2 \cdot 2\text{H}_2\text{O}$ . However, the weight loss of the sample is 25.82% at  $179.81^\circ\text{C}$ , which is lower than the theoretical value of 35.42%. It indicates that the product at this stage is not only  $\text{MgCl}_2 \cdot 2\text{H}_2\text{O}$  but also partially undecomposed  $\text{MgCl}_2 \cdot 4\text{H}_2\text{O}$ . When the temperature increased to  $289.23^\circ\text{C}$ , the sample decompose finally into a mixture of  $\text{MgOHCl} \cdot \text{H}_2\text{O}$  and  $\text{MgO}$ . The total weight loss of  $\text{MgCl}_2 \cdot 6\text{H}_2\text{O}$  is 58.07%. Except for the first weight loss corresponding to adsorbed air humidity (58.07% – 4.25% = 53.82%) is coincide with the theoretical value of 6 crystal waters (53.2%). For  $\text{NH}_4\text{Al}(\text{SO}_4)_2 \cdot 12\text{H}_2\text{O}$  (Figure 7b), the sample loses ten crystal waters in the first stage ( $93\sim 175^\circ\text{C}$ ) with the weight loss of 38.79%. In the second stage ( $175\sim 250^\circ\text{C}$ ), the sample continues to lose two crystal waters and the final weight loss is 47.43%. According to the experimental result, the value of crystal waters lost from the sample is calculated to be 11.8, which is almost equivalent to 12. Similar to  $\text{NH}_4\text{Al}(\text{SO}_4)_2 \cdot 12\text{H}_2\text{O}$ ,  $\text{KAl}(\text{SO}_4)_2 \cdot 12\text{H}_2\text{O}$  loses nine crystal waters at  $93.5\sim 200^\circ\text{C}$ , as illustrated in Figure 7c. When the temperature continues to increase

and exceeds 250 °C, the remaining three crystal waters are lost and the final weight loss is 44.01%. The error between experimental result and theoretic value (45.53%) is only 3.34%.

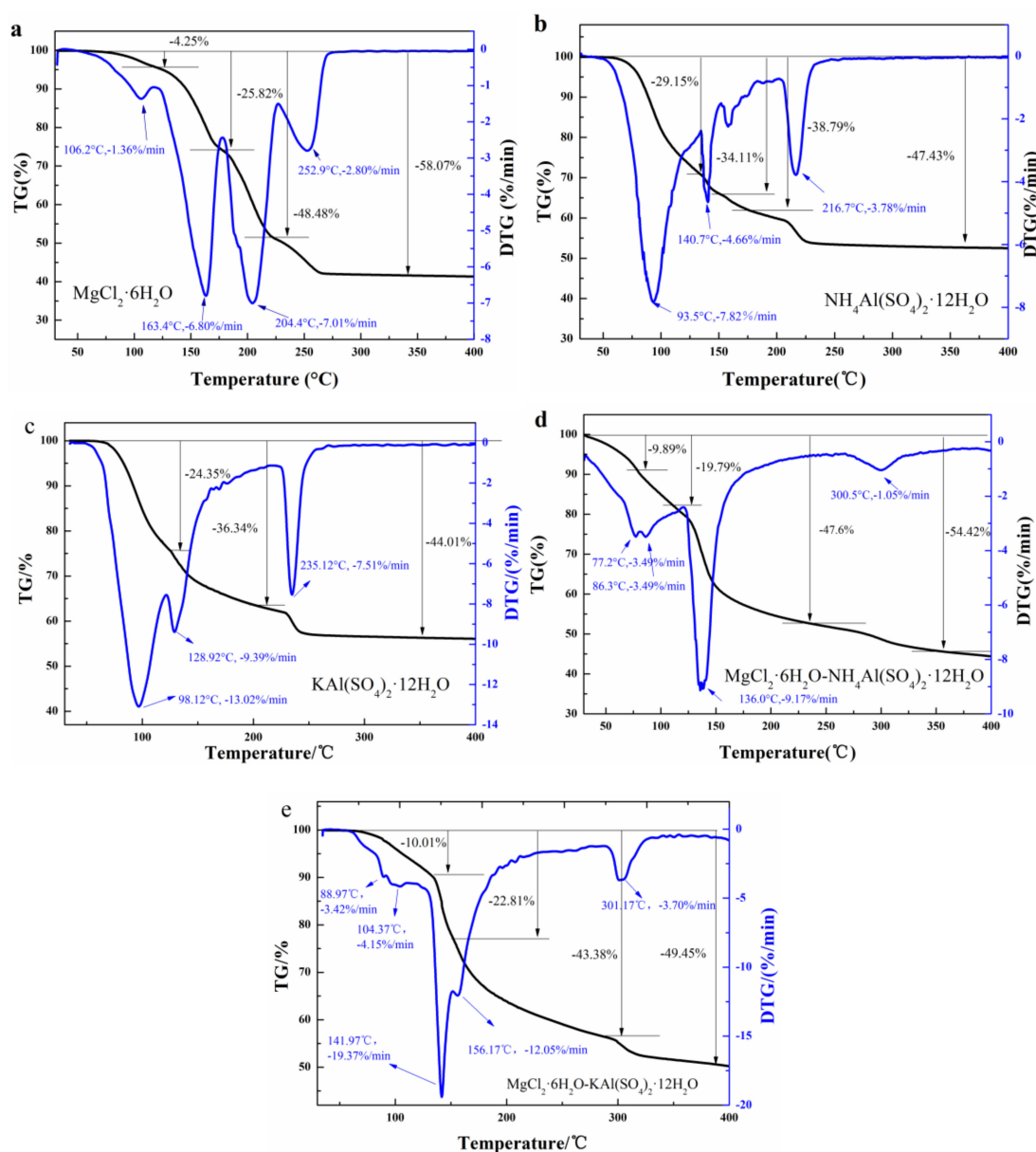


**Figure 7.** TGA curves of (a) MgCl<sub>2</sub>·6H<sub>2</sub>O, (b) NH<sub>4</sub>Al(SO<sub>4</sub>)<sub>2</sub>·12H<sub>2</sub>O, (c) KAl(SO<sub>4</sub>)<sub>2</sub>·12H<sub>2</sub>O, (d) mixture-A and (e) mixture-B.

As shown in Figure 7d, mixture-A (MgCl<sub>2</sub>·6H<sub>2</sub>O-NH<sub>4</sub>Al(SO<sub>4</sub>)<sub>2</sub>·12H<sub>2</sub>O) has multiple weight loss steps, which are different from those of MgCl<sub>2</sub>·6H<sub>2</sub>O and NH<sub>4</sub>Al(SO<sub>4</sub>)<sub>2</sub>·12H<sub>2</sub>O. In particular, the mixture exhibits a lower onset decomposition temperature as compared to its two components because of its lower phase change temperature (64.15 °C). Moreover, a weight loss of 19.79% occurred for the mixture at the temperature of 143.23 °C. The experimental results suggest that the thermal property of mixture-A is different from those of MgCl<sub>2</sub>·6H<sub>2</sub>O and NH<sub>4</sub>Al(SO<sub>4</sub>)<sub>2</sub>·12H<sub>2</sub>O, verifying the formation of the mixture between two components. It can be seen from Figure 7e that mixture-B has a similar process of weight loss as mixture-A. And the final weight loss (49.45%) of mixture-B (Figure 7e, MgCl<sub>2</sub>·6H<sub>2</sub>O-KAl(SO<sub>4</sub>)<sub>2</sub>·12H<sub>2</sub>O) is between those of MgCl<sub>2</sub>·6H<sub>2</sub>O (58.07%) and KAl(SO<sub>4</sub>)<sub>2</sub>·12H<sub>2</sub>O (44.01%).



### 2.3. Thermal Reliability of Mixture-A and Mixture-B

As we know, it is essential that PCM has good thermal reliability to undergo a number of thermal cycles. Therefore, the melting-freezing cycle test was carried out on mixture-A and mixture-B to investigate their thermal reliabilities. Figure 8 shows the DSC result of the mixture-A and mixture-B before and after experiencing different numbers of melting-freezing cycle tests. There is significant difference in thermal reliability between mixture-A and mixture-B. After 200 cycles of the melting-freezing cycle test, mixture-A exhibits a phase change temperature of 65.12 °C and a melting enthalpy of 189.28 kJ/kg (Figure 8a). Compared with the experimental result before the test, the deviations in phase change temperature and melting enthalpy are only 1.51% and 1.20%, respectively. However, the thermal property of mixture-B changes greatly with the increase in the number of cycles. As shown in Figure 8b, the melting enthalpy of mixture-B decreases to 101.3 kJ/kg after undergoing 30 cycles melting-freezing cycle tests. As mentioned in Section 2.2. Structure and thermal properties of the mixtures, the acicular crystals ( $\text{MgCl}_2 \cdot 6\text{H}_2\text{O}$ ) only stick to the surface of the octahedral crystal ( $\text{KAl}(\text{SO}_4)_2 \cdot 12\text{H}_2\text{O}$ ) while not connect two octahedral crystals. The lack of tight connection between the two crystals results in poor thermal reliability of mixture-B. Furthermore, the structure of mixture-B has changed after the cycling tests, as shown in Figure 9. The significant weakening of most of the diffraction peaks may be due to the reduction of  $\text{KAl}(\text{SO}_4)_2 \cdot 12\text{H}_2\text{O}$  in mixture-B. In fact,  $\text{NH}_4\text{Al}(\text{SO}_4)_2 \cdot 12\text{H}_2\text{O}$  and  $\text{KAl}(\text{SO}_4)_2 \cdot 12\text{H}_2\text{O}$  exhibit different thermal reliability although they have similar structures and properties. As shown in Table 3, the melting-freezing cycle tests of  $\text{NH}_4\text{Al}(\text{SO}_4)_2 \cdot 12\text{H}_2\text{O}$  and  $\text{KAl}(\text{SO}_4)_2 \cdot 12\text{H}_2\text{O}$  were carried out. It is found that the melting enthalpy of  $\text{KAl}(\text{SO}_4)_2 \cdot 12\text{H}_2\text{O}$  was reduced by more than 50% after 10 cycles of 60–105 °C. The large decrease in melting enthalpy may be because the poor reversibility of the combination of aluminum potassium sulfate and crystal waters. In this work, when the number of cycles reaches 10, the melting enthalpy of mixture-B decreases by 15.14% compared to the sample before the cycle test. It can be known that the combination of  $\text{MgCl}_2 \cdot 6\text{H}_2\text{O}$  and  $\text{KAl}(\text{SO}_4)_2 \cdot 12\text{H}_2\text{O}$  can improve the thermal reliability of  $\text{KAl}(\text{SO}_4)_2 \cdot 12\text{H}_2\text{O}$ . Nevertheless, mixture-B can't conform to requirements because the PCM is expected to be reused many times to reduce costs while 10 cycles are not enough. By comparison, the mixture-A with excellent thermal reliability is a promising material for practical applications.

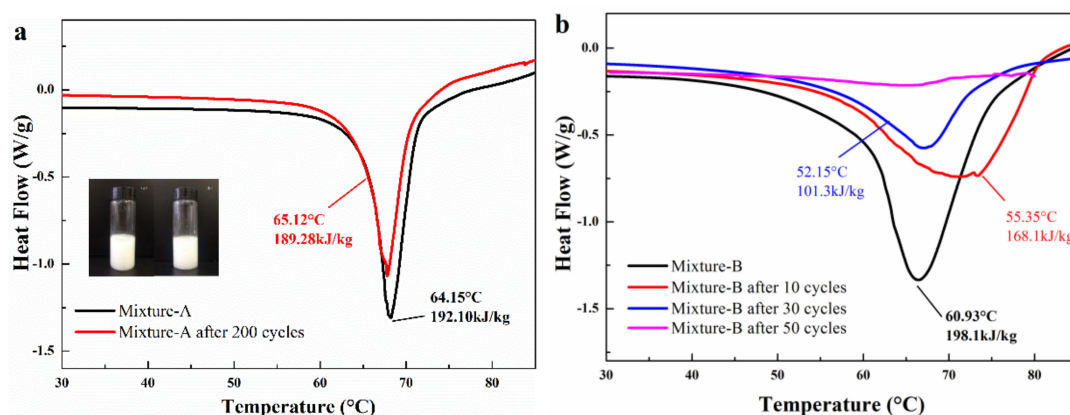
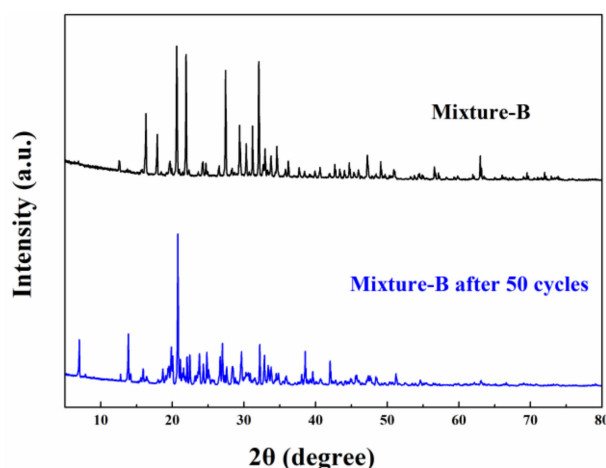


Figure 8. DSC result of (a) the mixture-A and (b) mixture-B before and after tests.



**Figure 9.** XRD patterns of Mixture-B before and after experiencing 50 heating-cooling cycles.

**Table 3.** Thermal reliability of  $\text{NH}_4\text{Al}(\text{SO}_4)_2 \cdot 12\text{H}_2\text{O}$  and  $\text{KAl}(\text{SO}_4)_2 \cdot 12\text{H}_2\text{O}$ .

	$\text{NH}_4\text{Al}(\text{SO}_4)_2 \cdot 12\text{H}_2\text{O}$		$\text{KAl}(\text{SO}_4)_2 \cdot 12\text{H}_2\text{O}$	
	$T_{\text{melt}}$ (°C)	$\Delta H$ (kJ/kg)	$T_{\text{melt}}$ (°C)	$\Delta H$ (kJ/kg)
0 cycles	93.86	264.0	90.85	261.3
After 5 cycles 60–105 °C	93.21	263.2	90.31	185.9
After 10 cycles 60–105 °C	93.50	251.0	91.83	107.3
After 20 cycles 60–105 °C	93.37	218.9	90.79	104.5

In order to ensure that the structure of the mixture-A didn't change after the cycle tests, XRD patterns and cooling curves before and after experiencing 200 melting-freezing cycles were measured. It can be seen from Figure 10a that the XRD patterns before and after the tests are almost the same, suggesting that the mixture-A has good structure stability. Moreover, the cooling curves of the mixture-A before and after the test almost coincide with each other (Figure 10b). It is revealed that the  $\text{MgCl}_2 \cdot 6\text{H}_2\text{O} \cdot \text{NH}_4\text{Al}(\text{SO}_4)_2 \cdot 12\text{H}_2\text{O}$  mixture possesses excellent thermal reliability, making it show great potentials for practical applications. In addition, the material expansion experiment result shows that the mixture A has no significant volume change before and after the phase change (Figure 10c).

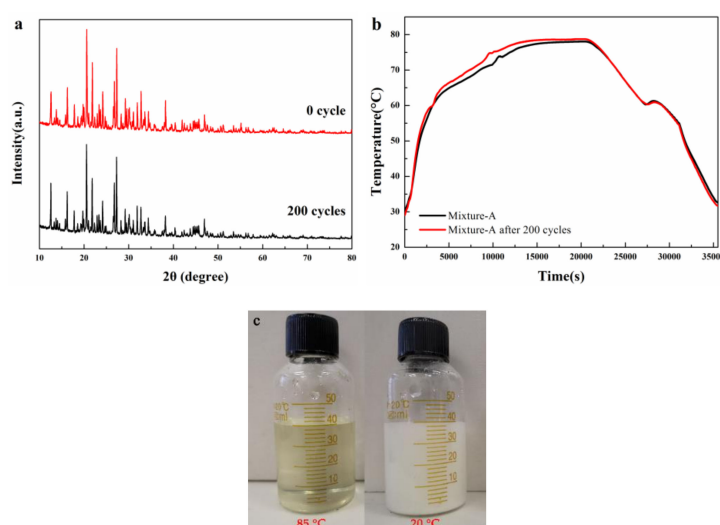


**Figure 10.** XRD patterns (a) and cooling curves (b) of the mixture-A before and after experiencing 200 heating-cooling cycles; and the material expansion test of mixture-A (c).

### 3. Materials and Methods

#### 3.1. Materials and Reagents

Magnesium chloride hexahydrate ( $\text{MgCl}_2 \cdot 6\text{H}_2\text{O}$ , AR), aluminum ammonium sulfate dodecahydrate ( $\text{NH}_4\text{Al}(\text{SO}_4)_2 \cdot 12\text{H}_2\text{O}$ , AR) and aluminum potassium sulfate dodecahydrate ( $\text{KAl}(\text{SO}_4)_2 \cdot 12\text{H}_2\text{O}$ , AR) were purchased from Guangzhou Chemical Reagent Factory (Guangzhou, China).

#### 3.2. Sample Preparation

##### 3.2.1. $\text{MgCl}_2 \cdot 6\text{H}_2\text{O}$ - $\text{NH}_4\text{Al}(\text{SO}_4)_2 \cdot 12\text{H}_2\text{O}$ Mixtures

A series of  $\text{MgCl}_2 \cdot 6\text{H}_2\text{O}$ - $\text{NH}_4\text{Al}(\text{SO}_4)_2 \cdot 12\text{H}_2\text{O}$  mixtures with different mass fractions of  $\text{MgCl}_2 \cdot 6\text{H}_2\text{O}$  were prepared for determining the mixture composition of  $\text{MgCl}_2 \cdot 6\text{H}_2\text{O}$  and  $\text{NH}_4\text{Al}(\text{SO}_4)_2 \cdot 12\text{H}_2\text{O}$ . The experimental steps are as follows: Firstly, the  $\text{MgCl}_2 \cdot 6\text{H}_2\text{O}$  and  $\text{NH}_4\text{Al}(\text{SO}_4)_2 \cdot 12\text{H}_2\text{O}$  were weighed and placed in a reagent bottle. After simply stirring the two hydrated salts, the mixture was heated to  $85\text{ }^\circ\text{C}$  and maintained for 3 h. Then, intermittent stirring was used to ensure uniform mixing of the two hydrated salts during heating process. Finally, the solution was cooled at room temperature to obtain a  $\text{MgCl}_2 \cdot 6\text{H}_2\text{O}$ - $\text{NH}_4\text{Al}(\text{SO}_4)_2 \cdot 12\text{H}_2\text{O}$  mixture.

##### 3.2.2. $\text{MgCl}_2 \cdot 6\text{H}_2\text{O}$ - $\text{KAl}(\text{SO}_4)_2 \cdot 12\text{H}_2\text{O}$ Mixtures

In order to determine the optimum content of  $\text{MgCl}_2 \cdot 6\text{H}_2\text{O}$ , a series of mixtures with different proportions of  $\text{MgCl}_2 \cdot 6\text{H}_2\text{O}$  and  $\text{KAl}(\text{SO}_4)_2 \cdot 12\text{H}_2\text{O}$  were prepared. The experimental steps are same as that for preparing  $\text{MgCl}_2 \cdot 6\text{H}_2\text{O}$ - $\text{NH}_4\text{Al}(\text{SO}_4)_2 \cdot 12\text{H}_2\text{O}$  mixture.

#### 3.3. Characterization

The phase change temperature and latent heat of the samples were measured using a differential scanning calorimeter (DSC, DSC Q20, TA Instruments, New Castle, DE, USA). For DSC measurements, 5–10 mg for every sample was sealed in an aluminum pan and heated from  $30\text{ }^\circ\text{C}$  to  $100\text{ }^\circ\text{C}$  at a heating rate of  $5\text{ }^\circ\text{C}/\text{min}$  under a constant stream of nitrogen at a flow rate of  $50\text{ mL}/\text{min}$ .

The structure of the sample was characterized by an X-ray diffraction (XRD, D8-ADVANCE, Bruker, Bruker, Billerica, MA, USA) using  $\text{Cu K}\alpha$  radiation ( $\lambda = 1.5406\text{ \AA}$ ). Diffraction patterns of the mixture were collected in the  $2\theta$  ranges from  $10^\circ$  to  $80^\circ$ .

The changes in morphology and microstructure the sample during crystallization were observed by using a polarization microscope (Observer.A1, Zeiss, Oberkochen, Germany). 30–50 mg of each sample was put on the glass slide to experience a temperature change from  $90\text{ }^\circ\text{C}$  to  $25\text{ }^\circ\text{C}$ .

In order to investigate the thermal stability of the mixture, the thermal gravimetric analysis of the samples were conducted by a thermoanalyzer instrument (TGA, STA409PC, Netzsch, Waldkraiburg, Germany). Each sample (8–12 mg) was placed in an alumina crucible and then heated from  $30$  to  $400\text{ }^\circ\text{C}$  at a heating rate of  $10\text{ }^\circ\text{C}/\text{min}$  under a constant stream of nitrogen at a flow rate of  $100\text{ mL}/\text{min}$ .

The thermal reliability of the mixture was tested by using the High-low temperature (alternate) humid heat test chamber (TH300, Shanghai Yiheng Scientific Instrument Co., Ltd., Shanghai, China). Before the melting-freezing cycle test, the mixture was sealed in a reagent bottle to avoid water loss. To ensure the reproducibility of experimental result, five samples (20–25 mg) were prepared for testing under the same cycle test conditions. The melting-freezing cycle experiment was carried out as following process: At first, the chamber was heated from room temperature to  $80\text{ }^\circ\text{C}$  at a rate of  $5\text{ }^\circ\text{C}/\text{min}$ . Then, the five samples were heated at  $80\text{ }^\circ\text{C}$  for 60 min to completely melt the mixture. After that, the chamber temperature decreased to  $30\text{ }^\circ\text{C}$  at a rate of  $5\text{ }^\circ\text{C}/\text{min}$ . Finally, the samples completely solidified after cooling 60 min at  $30\text{ }^\circ\text{C}$ . After repeating 200 cycles melting-freezing experiments, the samples were characterized by DSC and XRD to study the thermal reliability.

### 3.4. Measurement of Cooling Curves

As introduced in Section 3.3. Characterization, the mass of every DSC sample was controlled at 5–10 mg, which was much less than the mass of PCM used in the industry. Note that the sample amount, heating rate, sample compositions would interfere in the DSC signal [37–39]. In order to avoid the influence of small sample amount on PCM solidification temperature measurement, the measurement of T-history or cooling curve was widely used to determine the supercooling degree of PCM samples [40,41]. Therefore, the crystallization properties of the mixture samples in this work were characterized by measuring their cooling curves. Figure 11 shows a schematic diagram of the experimental setup, which consists of a thermostatic silicone oil bath box and a thermal energy storage (TES) unit. The silicone-oil bath could control the temperature automatically with an accuracy of  $\pm 0.01$  °C. And the TES unit used a cylindrical glass container with an inner diameter of 25 mm, a wall thickness of 1 mm and a length of 200 mm to place the sample. As shown in Figure 11, a K-type thermocouple was placed at the center of the cylindrical glass container to monitor the temperature change of each sample with a measurement error of  $\pm 0.1$  °C. Moreover, the test points were at the same depth (20 mm away from bottom of the container) in different tests, to make sure the effects of input heat flux from top and bottom on them were identical. On the other hand, two-third of the volume of the container was filled with the test sample, and the remaining space was left to adapt to the thermal expansion of the PCM. During the measurement, the TES unit was put into the oil bath and heated/cooled with the following program. Firstly, the oil was heated at a rate of 1 °C/min from the room temperature to the specified temperature (80 °C for mixtures, 105 °C for  $\text{NH}_4\text{Al}(\text{SO}_4)_2 \cdot 12\text{H}_2\text{O}$ /KAl(SO<sub>4</sub>)<sub>2</sub>·12H<sub>2</sub>O and 135 °C for  $\text{MgCl}_2 \cdot 6\text{H}_2\text{O}$ ). Secondly, the thermostatic silicone oil bath box was maintained at the specified temperature for 2 h until the samples completely melted. Finally, the oil was cooled down to 30 °C at a rate of 1 °C/min. At the same time, temperature data in the experiment was collected using a data logger (Agilent 34970A, Santa Clara, CA, USA).

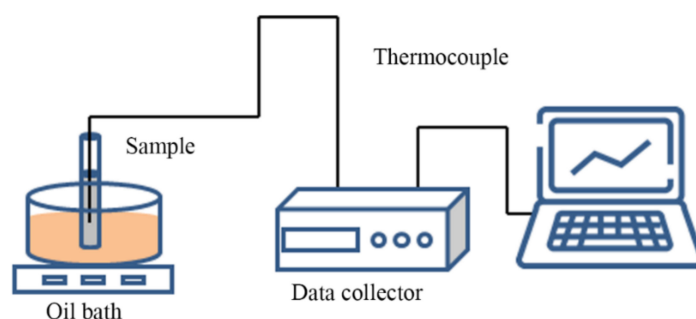


**Figure 11.** Schematic diagram of experimental setup for testing cooling curves.

## 4. Conclusions

Two series of mixtures (mixture-A:  $\text{MgCl}_2 \cdot 6\text{H}_2\text{O} \cdot \text{NH}_4\text{Al}(\text{SO}_4)_2 \cdot 12\text{H}_2\text{O}$  and mixture-B:  $\text{MgCl}_2 \cdot 6\text{H}_2\text{O} \cdot \text{KAl}(\text{SO}_4)_2 \cdot 12\text{H}_2\text{O}$ ) were investigated as PCMs for solar water heating system. The thermal property, structure and the thermal stability of PCM were studied systematically. The experimental results can be concluded as follows:

- 1) The mass fraction of  $\text{MgCl}_2 \cdot 6\text{H}_2\text{O}$  in mixture-A or mixture-B is determined to be 30 wt%. It is found that the mixture-A has a melting point of 64.15 °C, a melting enthalpy of 192.1 kJ/kg, and a very low supercooling degree (0.74 °C). On the other hand, the melting point and melting enthalpy of mixture-B without supercooling degree are 60.93 °C and 198.1 kJ/kg, respectively.
- 2) The XRD pattern of mixture-A shows that  $\text{MgCl}_2 \cdot 6\text{H}_2\text{O}$  and  $\text{NH}_4\text{Al}(\text{SO}_4)_2 \cdot 12\text{H}_2\text{O}$  combined physically and have no chemical reaction, like mixture-B ( $\text{MgCl}_2 \cdot 6\text{H}_2\text{O}$  and  $\text{KAl}(\text{SO}_4)_2 \cdot 12\text{H}_2\text{O}$ ).
- 3) The polarized microscope images show that the crystallization behaviors of mixture-A and mixture-B. The acicular crystals ( $\text{MgCl}_2 \cdot 6\text{H}_2\text{O}$ ) not only attach on the surface of the octahedral

crystals ( $\text{NH}_4\text{Al}(\text{SO}_4)_2 \cdot 12\text{H}_2\text{O}$ ) but also stick into the gaps between octahedral crystals. Furthermore, the free acicular crystals ( $\text{MgCl}_2 \cdot 6\text{H}_2\text{O}$ ) in the mixture-B eventually only adhere to the surface of the octahedral crystals ( $\text{KAl}(\text{SO}_4)_2 \cdot 12\text{H}_2\text{O}$ ).

- 4) The 200 heating-cooling cycle test reveals that the mixture-A possesses good structure stability and excellent thermal reliability while the mixture-B has poor thermal reliability. The suitable phase change temperature, high latent heat along with excellent thermal reliability make the  $\text{MgCl}_2 \cdot 6\text{H}_2\text{O}$ - $\text{NH}_4\text{Al}(\text{SO}_4)_2 \cdot 12\text{H}_2\text{O}$  mixture show great potential in solar water heating systems.
- 5) In conclusion, with a suitable melting point, high latent heat, good structure stability and excellent thermal reliability, mixture-A is a highly promising thermal energy storage phase change material for SWH system. In future work, the heat transfer efficiency of mixture-A and its compatibility with devices will require further research and exploration to better apply materials to practical SWH system or other thermal storage system.

**Author Contributions:** Conceptualization, Z.L. and Z.Z.; Data curation, W.S.; Investigation, W.S., Y.Z. and J.F.; Project administration, X.F. and Z.Z.; Writing—original draft, W.S. and Z.L.; Writing—review & editing, W.S. and Y.Z.

**Funding:** This research was funded by the National Natural Science Foundation of China (No. U1507201), the Joint Fund of Ministry of Education for Equipment Pre-Research (No. 6141A02022244) and the National Defense Basic Scientific Research Program of China (No. JCKY2018110C114).

**Conflicts of Interest:** The authors declare no conflict of interest.

## References

1. Alva, G.; Lin, Y.; Fang, G. An overview of thermal energy storage systems. *Energy* **2018**, *144*, 341–378. [[CrossRef](#)]
2. Farid, M.M.; Khudhair, A.M.; Razack, S.A.K.; Al-Hallaj, S. A review on phase change energy storage: Materials and applications. *Energ. Convers. Manag.* **2004**, *45*, 1597–1615. [[CrossRef](#)]
3. Zalba, B.; Marín, J.M.; Cabeza, L.F.; Mehling, H. Review on thermal energy storage with phase change: Materials, heat transfer analysis and applications. *Appl. Therm. Eng.* **2003**, *23*, 251–283. [[CrossRef](#)]
4. Sharma, A.; Tyagi, V.V.; Chen, C.R.; Buddhi, D. Review on thermal energy storage with phase change materials and applications. *Renew. Sust. Energ. Rev.* **2009**, *13*, 318–345. [[CrossRef](#)]
5. Mohamed, S.A.; Al-Sulaiman, F.A.; Ibrahim, N.I.; Zahir, M.H.; Al-Ahmed, A.; Saidur, R.; Yılbaş, B.S.; Sahin, A.Z. A review on current status and challenges of inorganic phase change materials for thermal energy storage systems. *Renew. Sust. Energ. Rev.* **2017**, *70*, 1072–1089. [[CrossRef](#)]
6. Sun, W.C.; Huang, R.; Ling, Z.Y.; Fang, X.M.; Zhang, Z.G. Two types of composite phase change panels containing a ternary hydrated salt mixture for use in building envelope and ventilation system. *Energ. Convers. Manag.* **2018**, *177*, 306–314. [[CrossRef](#)]
7. Sun, Z.; Zhang, Y.; Zheng, S.; Park, Y.; Frost, R.L. Preparation and thermal energy storage properties of paraffin/calcined diatomite composites as form-stable phase change materials. *Therm. Acta* **2013**, *558*, 16–21. [[CrossRef](#)]
8. Özonur, Y.; Mazman, M.; Paksoy, H.Ö.; Evliya, H. Microencapsulation of coco fatty acid mixture for thermal energy storage with phase change material. *Int. J. Energ. Res.* **2006**, *30*, 741–749. [[CrossRef](#)]
9. Alper Aydın, A. High-chain fatty acid esters of 1-octadecanol as novel organic phase change materials and mathematical correlations for estimating the thermal properties of higher fatty acid esters' homologous series. *Sol. Energ. Mater. Sol. Cells* **2013**, *113*, 44–51. [[CrossRef](#)]
10. Alkan, C.; Sari, A. Fatty acid/poly(methyl methacrylate) (PMMA) blends as form-stable phase change materials for latent heat thermal energy storage. *Sol. Energ.* **2008**, *82*, 118–124. [[CrossRef](#)]
11. Li, G.; Zhang, X.; Wang, J.; Fang, J. From anisotropic graphene aerogels to electron- and photo-driven phase change composites. *J. Mater. Chem. A* **2016**, *4*, 17042–11704. [[CrossRef](#)]
12. Ye, R.; Zhang, C.; Sun, W.; Fang, X.; Zhang, Z. Novel wall panels containing  $\text{CaCl}_2 \cdot 6\text{H}_2\text{O}$ - $\text{Mg}(\text{NO}_3)_2 \cdot 6\text{H}_2\text{O}$ /expanded graphite composites with different phase change temperatures for building energy savings. *Energ. Buildings* **2018**, *176*, 407–417. [[CrossRef](#)]

13. da Cunha, J.P.; Eames, P. Thermal energy storage for low and medium temperature applications using phase change materials—A review. *Appl. Energ.* **2016**, *177*, 227–238. [[CrossRef](#)]
14. Gasia, J.; Miró, L.; Cabeza, L.F. Review on system and materials requirements for high temperature thermal energy storage. Part 1: General requirements. *Renew. Sustain. Energ. Rev.* **2017**, *75*, 1320–1338. [[CrossRef](#)]
15. Sharma, A.; Chen, C.R. Solar water heating system with phase change materials. *Int. Rev. Chem. Eng. Rapid Comm.* **2009**.
16. Sari, A.; Biçer, A. Preparation and thermal energy storage properties of building material-based composites as novel form-stable PCMs. *Energ. Buildings* **2012**, *51*, 73–83. [[CrossRef](#)]
17. Zhou, G.; Yang, Y.; Wang, X.; Zhou, S. Numerical analysis of effect of shape-stabilized phase change material plates in a building combined with night ventilation. *Appl. Energ.* **2009**, *86*, 52–59. [[CrossRef](#)]
18. Zhou, D.; Zhao, C.Y.; Tian, Y. Review on thermal energy storage with phase change materials (PCMs) in building applications. *Appl. Energ.* **2012**, *92*, 593–605. [[CrossRef](#)]
19. Lane, G.A. Phase change materials for energy storage nucleation to prevent supercooling. *Sol. Energ. Mater. Sol. Cells* **1992**, *27*, 135–160. [[CrossRef](#)]
20. Hu, P.; Lu, D.-J.; Fan, X.-Y.; Zhou, X.; Chen, Z.-S. Phase change performance of sodium acetate trihydrate with AlN nanoparticles and CMC. *Sol. Energ. Mater. Sol. Cells* **2011**, *95*, 2645–2649. [[CrossRef](#)]
21. Garay Ramirez, B.M.L.; Glorieux, C.; San Martin Martinez, E.; Flores Cuautle, J.J.A. Tuning of thermal properties of sodium acetate trihydrate by blending with polymer and silver nanoparticles. *Appl. Therm. Eng.* **2014**, *62*, 838–844. [[CrossRef](#)]
22. Ze-Shao, L.D.-J.H.P.Z.B.-B.L.Y.C. Study on the performance of nanoparticles as nucleating agents for sodium acetate trihydrate. *J. Eng. Thermophys.* **2012**, *33*, 1279–1282.
23. Li, G.; Zhang, B.; Li, X.; Zhou, Y.; Sun, Q.; Yun, Q. The preparation, characterization and modification of a new phase change material:  $\text{CaCl}_2 \cdot 6\text{H}_2\text{O}$ - $\text{MgCl}_2 \cdot 6\text{H}_2\text{O}$  eutectic hydrate salt. *Sol. Energ. Mater. Sol. Cells* **2014**, *126*, 51–55. [[CrossRef](#)]
24. Mao, J.; Dong, X.; Hou, P.; Lian, H. Preparation research of novel composite phase change materials based on sodium acetate trihydrate. *Appl. Therm. Eng.* **2017**, *118*, 817–825. [[CrossRef](#)]
25. Mao, J.; Hou, P.; Liu, R.; Chen, F.; Dong, X. Preparation and thermal properties of SAT-CMC-DSP/EG composite as phase change material. *Appl. Therm. Eng.* **2017**, *119*, 585–592. [[CrossRef](#)]
26. Li, T.X.; Wu, D.L.; He, F.; Wang, R.Z. Experimental investigation on copper foam/hydrated salt composite phase change material for thermal energy storage. *Int. J. Heat Mass Transf.* **2017**, *115*, 148–157. [[CrossRef](#)]
27. Yuan, K.; Zhou, Y.; Sun, W.; Fang, X.; Zhang, Z. A polymer-coated calcium chloride hexahydrate/expanded graphite composite phase change material with enhanced thermal reliability and good applicability. *Compos. Sci. Technol.* **2018**, *156*, 78–86. [[CrossRef](#)]
28. Ye, R.; Lin, W.; Fang, X.; Zhang, Z. A numerical study of building integrated with  $\text{CaCl}_2 \cdot 6\text{H}_2\text{O}$ /expanded graphite composite phase change material. *Appl. Therm. Eng.* **2017**, *126*, 480–488. [[CrossRef](#)]
29. Karaipekli, A.; Sari, A. Capric-myristic acid/expanded perlite composite as form-stable phase change material for latent heat thermal energy storage. *Renew. Energ.* **2008**, *33*, 2599–2605. [[CrossRef](#)]
30. Fu, L.; Wang, Q.; Ye, R.; Fang, X.; Zhang, Z. A calcium chloride hexahydrate/expanded perlite composite with good heat storage and insulation properties for building energy conservation. *Renew. Energ.* **2017**, *114*, 733–743. [[CrossRef](#)]
31. Konuklu, Y.; Ersoy, O.; Gokce, O. Easy and industrially applicable impregnation process for preparation of diatomite-based phase change material nanocomposites for thermal energy storage. *Appl. Therm. Eng.* **2015**, *91*, 759–766. [[CrossRef](#)]
32. Jeong, S.-G.; Jeon, J.; Lee, J.-H.; Kim, S. Optimal preparation of PCM/diatomite composites for enhancing thermal properties. *Int. J. Heat Mass Transf.* **2013**, *62*, 711–717. [[CrossRef](#)]
33. Nagano, K.; Ogawa, K.; Mochida, T.; Hayashi, K.; Ogoshi, H. Thermal characteristics of magnesium nitrate hexahydrate and magnesium chloride hexahydrate mixture as a phase change material for effective utilization of urban waste heat. *Appl. Therm. Eng.* **2004**, *24*, 221–232. [[CrossRef](#)]
34. Liu, Y.; Yang, Y. Use of nano- $\alpha\text{-Al}_2\text{O}_3$  to improve binary eutectic hydrated salt as phase change material. *Sol. Energ. Mater. Sol. Cells* **2017**, *160*, 18–25. [[CrossRef](#)]
35. Nagano, K.; Ogawa, K.; Mochida, T.; Hayashi, K.; Ogoshi, H. Performance of heat charge/discharge of magnesium nitrate hexahydrate and magnesium chloride hexahydrate mixture to a single vertical tube for a latent heat storage system. *Appl. Therm. Eng.* **2004**, *24*, 209–220. [[CrossRef](#)]

36. Ding, Q.; Luo, X.; Lin, X.; Zhang, H. Study of magnesium nitrate hexahydrate and magnesium chloride hexahydrate mixture as phase change material. In Proceedings of the Asia-Pacific Power and Energy Engineering Conference (APPEEC), Sabah, Malaysia, 7–10 October 2018; 2012; pp. 1–4.
37. Sole, A.; Miro, L.; Barreneche, C.; Martorell, I.; Cabeza, L.F. Review of the T-history method to determine thermophysical properties of phase change materials (PCM). *Renew. Sust. Energ. Rev.* **2013**, *26*, 425–436. [[CrossRef](#)]
38. Gunther, E.; Hiebler, S.; Mehling, H.; Redlich, R. Enthalpy of Phase Change Materials as a Function of Temperature: Required Accuracy and Suitable Measurement Methods. *Int. J. Thermophys.* **2009**, *30*, 1257–1269. [[CrossRef](#)]
39. Castellon, C.; Gunther, E.; Mehling, H.; Hiebler, S.; Cabeza, L.F. Determination of the enthalpy of PCM as a function of temperature using a heat-flux DSC-A study of different measurement procedures and their accuracy. *Int. J. Energ. Res.* **2008**, *32*, 1258–1265. [[CrossRef](#)]
40. Chiu, J.N.W.; Martin, V. Submerged finned heat exchanger latent heat storage design and its experimental verification. *Appl. Energ.* **2012**, *93*, 507–516. [[CrossRef](#)]
41. Zhou, G.B.; Xiang, Y.T. Experimental investigations on stable supercooling performance of sodium acetate trihydrate PCM for thermal storage. *Sol. Energ.* **2017**, *155*, 1261–1272. [[CrossRef](#)]

**Sample Availability:** Samples of the compounds are not available from the authors.



© 2019 by the authors. Licensee MDPI, Basel, Switzerland. This article is an open access article distributed under the terms and conditions of the Creative Commons Attribution (CC BY) license (<http://creativecommons.org/licenses/by/4.0/>).